JCTC Journal of Chemical Theory and Computation

Article

pubs.acs.org/JCTC

GolP-CHARMM: First-Principles Based Force Fields for the Interaction of Proteins with Au(111) and Au(100)

Louise B. Wright,[†] P. Mark Rodger,[†] Stefano Corni,*[,‡] and Tiffany R. Walsh*[,§]

[†]University of Warwick, Dept. of Chemistry and Centre for Scientific Computing, Coventry, CV4 7AL, United Kingdom

[‡]Centro S3, CNR Istituto Nanoscienze, Modena, Italy

[§]Deakin University, Institute for Frontier Materials, Geelong, Vic. 3216, Australia

Supporting Information

ABSTRACT: Computational simulation of peptide adsorption at the aqueous gold interface is key to advancing the development of many applications based on gold nanoparticles, ranging from nanomedical devices to smart biomimetic materials. Here, we present a force field, GolP-CHARMM, designed to capture peptide adsorption at both the aqueous Au(111) and Au(100) interfaces. The force field, compatible with the bio-organic force field CHARMM, is parametrized using a combination of experimental and first-principles data. Like its predecessor, GolP (Iori, F.; et al. *J. Comput. Chem.* **2009**, *30*, 1465), this force field contains terms to describe the dynamic polarization of gold atoms, chemisorbing species, and the interaction between sp^2 hybridized carbon atoms and gold. A systematic study of small molecule adsorption at both surfaces using the vdW-DF functional (Dion, M.; et al. *Phys. Rev. Lett.* **2004**, *92*, 246401−1. Thonhauser, T.; et al. *Phys. Rev. B* **2007**, *76*, 125112) is carried out to fit and test force field parameters and also, for the first time, gives unique insights into facet selectivity of gold binding *in vacuo*. Energetic and spatial trends observed in our DFT calculations are reproduced by the force field under the same conditions. Finally, we use the new force field to calculate adsorption energies, under aqueous conditions, for a representative set of amino acids. These data are found to agree with experimental findings.

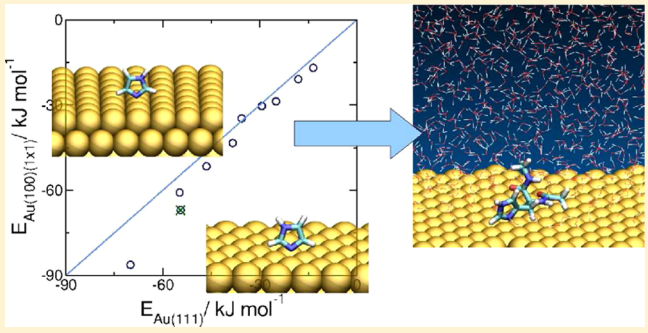

INTRODUCTION

The aqueous biomolecule−gold interface is of increasing interest to a range of different cross-disciplinary areas of science, including biomimetic materials synthesis[1−3] and nanomedicine.[4−7] For example, the narrow, intense plasmon adsorption bands of gold nanoparticles (AuNPs) make AuNPs ideal candidates as biomedical probes for cancer diagnostics or therapeutics,[4−6,8] if functionalized by the appropriate proteins. Alongside medicinal applications, the use of biomolecules to direct the organization of AuNPs into specific multifunctional nanostructures offers a promising route for the rational design of new materials with predefined properties.[9−15] Experimental determination of biomolecule conformation and/or aggregation, upon adsorption to either planar gold surfaces or AuNPs, remains challenging, despite recent advances.[16,17] However, such information is key to advancing the development of biofunctionalized AuNP applications, both in the realm of bionanomedicine and biomimetics. Molecular simulation, in partnership with experiment, is an essential tool for making such advances.

In recent years, several groups have probed biomolecule−gold adsorption under aqueous conditions using atomistic molecular dynamics (MD).[18−31] Key to the success of such simulations is the ability of the force field (FF) used to capture the essential physics and chemistry of the system. At present, two FFs have found widespread adoption for studying peptide adsorption via simulations at the aqueous gold interface: CHARMM-METAL (also compatible with CVFF and a number of other biomolecular FFs),[32] which was parametrized to reproduce bulk metal density and surface tension, and GolP[33,34] (compatible with OPLS-AA[35]), which was specifically targeted to protein−surface interactions. The latter FF also includes terms to describe the dynamic polarization of gold atoms induced by biomolecule adsorption. Covalent interactions with gold, such as the dynamic formation and dissociation of a thiol S−H bond,[36,37] are not within the scope of most atomistic MD approaches and hence are not modeled by either of these two FFs. The inert nature of planar gold surfaces, however, makes this surface a suitable candidate for a nonreactive biointerfacial FF.

With interest in the biomimetic community turning toward facet selectivity of biomolecule adsorption,[19,26,38] FFs parametrized on an equal footing for a range of gold surfaces are needed. While several groups have used the CVFF/CHARMM-METAL FF (in which the parameters are not restricted to any specific gold facet) to study differences in peptide adsorption onto the Au(111) and Au(100) planar surfaces or the surface of

Received: November 19, 2012
Published: January 29, 2013

 © 2013 American Chemical Society

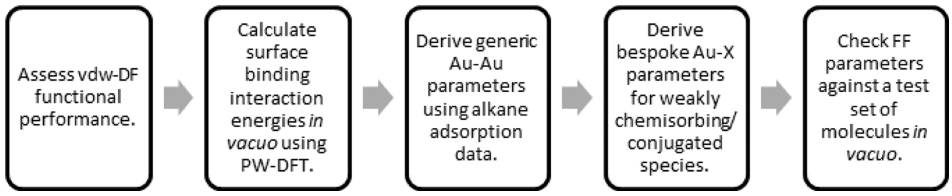

Figure 1. Scheme depicting the steps taken to parametrize the Au(111) and Au(100) surfaces.

a AuNP,[19,20,24−26] the dynamic polarization of the metal atoms was neglected in these works. Recently, calculations carried out *a posteriori* on MD simulations employing CVFF-METAL[20] revealed that on surfaces such as Au(100), where the epitaxial match between a biomolecule and underlying gold atoms was poor, the energy associated with the image-charge effect was significant. Another limitation of the CHARMM/CVFF-METAL potential is that it was not specifically parametrized to capture individual molecule−gold interactions and thus does not include terms to account for the weak chemisorption of the sulfur- and nitrogen-containing functional groups present in peptides. On the other hand, while the GolP FF accounts for polarization of the metal atoms and had been parametrized for all the interactions found in peptides, it is presently restricted to the Au(111) surface.

In this paper, we extend the GolP FF to describe peptide adsorption on the Au(100) surface, as well as the Au(111) surface. Our new FF will hence enable the phenomenon of facet-selective peptide adsorption on AuNPs to be investigated while accounting for gold atom polarization, since the Au(111) and Au(100) surfaces are the most commonly featured facets of AuNPs.[39] We have also chosen to reparametrize the Au(111) surface to make the new FF (herein denoted "GolP-CHARMM") compatible with the CHARMM FF.[40−42] Although refinement of bio-organic FFs is a rapidly advancing area of research, a number of studies have shown that the most recent version of CHARMM (CHARMM22*[42]) performs well for predicting the structure of proteins and peptides in solution.[42−45] While some have questioned whether biomolecule FF parameters derived for solution based studies are directly transferable to biointerfacial simulations,[43,46] a FF for gold that is consistent with an existing bio-organic FF, such as CHARMM, remains the only viable way to predict peptide adsorption equilibria from computational simulations.

A number of the key features of GolP have been incorporated into the current work. In particular, GolP-CHARMM has been parametrized with respect to experimental and first-principles data to capture biomolecule adsorption. As for GolP, the dynamic polarizability of gold atoms in our model is described using an ensemble of rigid rods.[34] This empirical model has been shown not only to be a computationally efficient method for incorporating the image charge effect in planar interfacial metal FFs[33,47,48] but also to be physically realistic.[34] In addition, the general concept that inclusion of polarization can facilitate transferability of parameters derived in the gas phase to the condensed phase is well-known (e.g., the AMOEBA FF[49]). Thus, GolP-CHARMM parameters, fit to *in vacuo* reference data, are suitable for the study of peptide adsorption onto gold under *aqueous* conditions. However, we emphasize that the parameters detailed in this work are not transferable to gold surfaces outside Au(111) and Au(100).

Surface reconstruction in the two facets modeled here, Au(111) and Au(100), has not been accounted for. While for Au(111) only marginally small differences exist between the structures of the reconstructed $22x\sqrt{3}$ and ideal surfaces,[50] the same is not true for Au(100). Experimentally, it has been shown that the adsorption of some small molecules, containing functional groups that are also present in biomolecules, onto Au(100) can promote[51] the Au(100)-*hex* reconstruction[52−54] under aqueous conditions, while others stabilize the ideal surface.[55] Hence, it is possible that the structure of the Au(100) surface local to an adsorbed biomolecule has the ideal Au(100) (1×1) structure. The role of surface reconstruction on biomolecule adsorption is yet to be investigated fully, and in the case of AuNPs featuring Au(100) facets, it is unknown whether the surface is native or reconstructed.

The FF reported in this work has been constructed to capture the peptide−gold interaction. The gold atoms in GolP-CHARMM are held frozen in their ideal bulk lattice positions, and hence the intra-gold interaction remains undetermined for our gold surfaces. Although this makes GolP-CHARMM unsuitable for modeling the properties of the gold lattice itself, i.e., in the calculation of interfacial surface energies, the previous biointerfacial FFs for gold in which the surface atoms are mobile present other complications; e.g., the reconstructed Au(100)-*hex* surface is found to be significantly unstable relative to the unreconstructed Au(100)(1 × 1) surface.[21,32,56,57] In addition, our Plane Wave-Density Functional Theory (PW-DFT) calculations revealed negligible relaxation of the gold surface upon small molecule adsorption.

In this paper, we report the results of two different sets of MD simulations designed to test our new FF parameters. First, the solvated Au(111) and Au(100)(1×1), herein denoted simply as "Au(100)," interfaces were studied to probe facet selective differences in the structure of interfacial water molecules under aqueous conditions. Second, trends in the surface binding energies (again under aqueous conditions) of amino acids, featuring a range of different functional groups, have been compared with experimental data.[58]

METHODS

In GolP-CHARMM, the potential energy function for the interaction between the gold surface and a biomolecule is[33]

$$V^{\mathrm{tot}}_{\mathrm{Au-X}} = V^{\mathrm{im}}_{\mathrm{Au-X}} + V^{\mathrm{vdW}}_{\mathrm{Au-X}} + V^{\mathrm{chemisorb}}_{\mathrm{Au-X}} + V^{\pi}_{\mathrm{Au-X}} \quad (1)$$

where $V^{\mathrm{im}}_{\mathrm{Au-X}}$ is the Coulombic electrostatic interaction between the biomolecule and the image charges it induces in the gold upon adsorption, and $V^{\mathrm{vdW}}_{\mathrm{Au-X}}$, $V^{\mathrm{chemisorb}}_{\mathrm{Au-X}}$, and $V^{\pi}_{\mathrm{Au-X}}$ are the van der Waals, chemisorption, and π electron interactions between the biomolecule and gold. A dynamic ensemble of rigid rods (described elsewhere[34]), each with a small dipole, has been used to capture image charge effects, while van der Waals interactions are described by the 12−6 Lennard-Jones (LJ) potential (eq 2). LJ parameters for gold atoms ($\sigma_{\mathrm{Au-Au}}$, $\varepsilon_{\mathrm{Au-Au}}$), when combined with LJ parameters from biomolecule atom types, were fitted to reproduce either experimental or PW-DFT interaction energies. Since the gold atoms are immobile in the

dx.doi.org/10.1021/ct301018m | J. Chem. Theory Comput. 2013, 9, 1616−1630

FF, the Au−Au terms are not needed to model the gold directly but only to define cross-terms with atoms from the interacting biomolecules. In accordance with CHARMM, the Lorentz−Berthelot mixing rules ($\sigma_{ij} = (\sigma_i + \sigma_j)/2$, $\varepsilon_{ij} = (\varepsilon_i \times \varepsilon_j)^{1/2}$) are used here,[59] where

$$V^{\mathrm{vdW}}(r_{ij}) = 4\varepsilon_{ij}\left[\left(\frac{\sigma_{ij}}{r_{ij}}\right)^{12} - \left(\frac{\sigma_{ij}}{r_{ij}}\right)^{6}\right] \quad (2)$$

A multiscale approach has been adopted, as reported previously by delle Site and co-workers,[60,61] and is summarized in Figure 1. In any FF there must be a balance between chemical and physical veracity and computational efficiency. For the FFs described herein, we have chosen to sacrifice some generality in order to capture a more detailed resolution of the key surfaces. While at the first-principles level of theory interactions between atoms in an adsorbing species and gold are unique to both each atom in question and its chemical environment in the adsorbate, we found that only a limited number of different Au−X (X = any atom) parameters were necessary in our FF; cross-terms derived for one species were often transferable to similar molecules, via the mixing rules. For each surface, Au(111) and Au(100), generic LJ parameters for gold (denoted "Au−Au") were fitted to reproduce alkane adsorption energies. Specific Au−X (X = S, N, O, H(−O), and C in carbon−carbon multiple bonds) LJ terms have then been derived for weakly chemisorbing species and sp^2 hybridized carbon systems (by which we mean aromatic rings and C═C bonds, both isolated and conjugated), using small molecules containing the same functional groups present in peptides. While in the original GolP these terms were added for Au−S and Au−N interactions only, this has been extended in the present work to also include Au−O and Au−H(O). In this work, GolP-CHARMM has been fitted to reproduce the adsorbed geometry and energetics of single water molecules using PW-DFT data. This contrasts with both GolP and CHARMM-METAL, neither of which have been parametrized against gold−water interactions.

Experimental data for alkane adsorption, from which LJ parameters can be derived, is only available for the Au(111) surface. Hence, in order to extend GolP to gold surfaces other than Au(111), we have used PW-DFT calculations. Here, the van der Waals Density Functional (vdW-DF),[62−64] combined with the revised Perdew−Burke−Ernzerhof (revPBE)[65] functional, has been employed; this has been shown to reproduce dispersion interactions reasonably well. First, we assessed the suitability of this functional for describing small molecule−gold adsorption by comparing experimental and calculated interaction energies for a number of different functional groups on Au(111) (Figure 2). Our FF LJ parameters for the Au(111) surface were fitted to a combination of experimental and calculated interaction energies (Table S1); in the absence of appropriate experimental data, LJ terms for Au(100) were fitted to calculated interaction energies only.

A unique feature of GolP is the presence of virtual sites on the Au(111) surface to direct "atop" Au atom adsorption (by "atop" we mean that the heteroatom is preferentially adsorbed directly above a real Au atom in the surface, rather than above a hollow or bridge surface site) as observed in first-principles calculations.[33,66,67] It is the virtual sites, and not the real gold surface atoms, that have spatial extent and interact with adsorbing species via the LJ terms; while dipolar rods are located on each gold atom. Without employing this scheme,

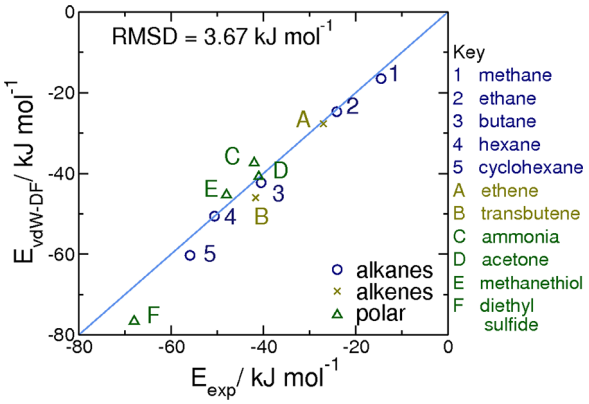

Figure 2. Correlation between experimental interaction energies for small molecules adsorbed onto the Au(111) surface and those calculated with vdW-DF.[62−64]

adsorption occurs away from atop Au sites when van der Waals interactions are described by a LJ potential. The same virtual site geometry used previously has been adopted here for the Au(111) surface[33] (Figure 3a). In the case of the Au(100) surface, a number of different virtual site geometries have been tested (Figure S1); the optimal arrangement is shown in Figure 3b.

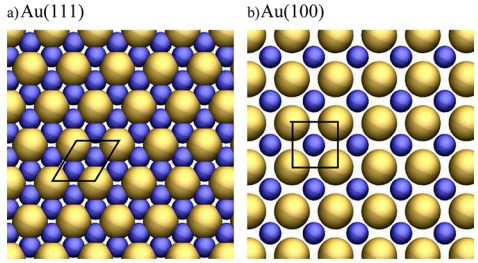

Figure 3. Arrangement of virtual sites on (a) the Au(111) and (b) the Au(100) surface. Real gold surface atoms are shown in gold, virtual sites in blue.

FORCE-FIELD PARAMETRIZATION

Plane Wave DFT Calculations. PW-DFT calculations have been carried out for the molecules listed in Table 1 adsorbed onto the Au(111) and Au(100) surfaces *in vacuo*, using Quantum Espresso (versions 4.3.x).[68] Three-dimensional periodic boundary conditions were employed, with supercell dimensions (Table 1, Au−Au lattice parameter of 2.93 Å[69]) and vacuum thickness in the direction normal to the surface chosen to ensure interactions between periodic images were insignificant.[33] Gold slabs four and five atomic layers thick were used for the Au(111) and Au(100) surfaces, respectively. Calculations were performed using vdW-DF[62−64] with the revPBE exchange-correlation functional[65] and ultrasoft pseudopotentials[70] (derived using the PBE exchange-correlation functional[69,71]) to describe electron-ion interactions. Plane wave kinetic energies and electron densities were truncated at 25 and 200 Ry, respectively. Brillouin zone integration was carried out using a Gaussian smearing technique[72] with a width of 0.05 Ry.

Optimal adsorbate−gold geometries were obtained by relaxing the structure of each small molecule when in close proximity to the surface (to a convergence criterion of 0.026 eV/Å). In the case of the Au(111) surface, favorable

Table 1. Surface Supercell Dimensions Used in PW-DFT Calculations for Each of the Small Molecules Investigated[a]

molecule	Au(111) supercell	Au(100) supercell
methane	$2\sqrt{3} \times 3$	3×3
ethane	$2\sqrt{3} \times 3$	n/a
butane	$2\sqrt{3} \times 3$	4×4
hexane	$3 \times 3\sqrt{3}$	n/a
cyclohexane	$2\sqrt{3} \times 4$	n/a
ethene	$2\sqrt{3} \times 3$	3×3
trans-but-2-ene	$2\sqrt{3} \times 3$	4×4
acetone	$2\sqrt{3} \times 3$	n/a
diethyl sulfide	$3 \times 3\sqrt{3}$	4×4
ammonia	$2\sqrt{3} \times 3$	3×3
imidazole	$2\sqrt{3} \times 3$	4×4
CH_3SH	$2\sqrt{3} \times 3$	3×3
water	$2\sqrt{3} \times 3$	3×3
methanol	$2\sqrt{3} \times 3$	3×3
methyl amide	$2\sqrt{3} \times 3$	3×3
methyl amine	$2\sqrt{3} \times 3$	3×3
methanoic acid	$2\sqrt{3} \times 3$	3×3
phenol	n/a	4×4
indole	n/a	4×4
toluene	n/a	4×4
methyl sulfide	n/a	3×3
ethanthiol	n/a	3×3
benzene	n/a	4×4

[a]Four and five atomic layers of gold were used for the Au(111) and Au(100) surfaces, respectively. n/a denotes where calculations were not performed.

configurations found from the previous study (which employed the PBE functional only) were used as the starting point for the work here. For Au(100), a number of initial geometries were tested, differing in both molecular orientation in space (e.g., with plane or key bonds oriented either perpendicular or parallel to the surface normal) and position relative to the underlying gold lattice (e.g., heteroatoms placed above top, hollow and bridge Au atom sites). A vacuum thickness of 10 Å and a Monkhorst–Pack k-point mesh of $4 \times 4 \times 1$ were used in all geometry optimization calculations.

Interaction energies of the small molecules listed in Table 1 with the Au(111) and Au(100) surfaces were calculated as follows:

$$\Delta E_{\text{mol\_Au}} = E_{\text{mol\_Au}} - E_{\text{mol}} - E_{\text{Au}} \quad (3)$$

where $E_{\text{mol\_Au}}$, E_{mol}, and E_{Au} are the total energies of systems describing the small molecule adsorbed at the interface, the adsorbate only, and the gold slab only, respectively. All three cells were relaxed, as described above, with optimal geometries being used in a single point calculation to determine the total energy. A thicker vacuum layer of 25 Å and a finer Monkhorst–Pack k-point mesh of $6 \times 8 \times 1/8 \times 8 \times 1$ (Au(111)/Au(100)) were employed in these single-point calculations. Interaction energies calculated using this "compartmentalization" method differed minimally from those computed as the difference between the total energies of the entire system with the small molecule adsorbed on the surface and free in the center of the cell.

***In Vacuo* Force-Field Calculations.** All FF-based calculations were performed using the Molecular Dynamics (MD) simulation package, Gromacs[73] version 4.5.4. Gold slabs of surface areas 29.3×30.4 Å^2 and 29.3×29.3 Å^2 (both five layers thick) were used for the Au(111) and Au(100) surfaces, respectively. Three dimensional periodic boundary conditions were employed in all calculations using cells with a z dimension of 70 Å; the vacuum layer between the adsorbed molecule and the nearest periodic image of the slab was approximately 60 Å. The calculations were carried out in the *NVT* ensemble with the temperature maintained using a Nosé–Hoover thermostat. Particle Mesh Ewald (PME) electrostatic summation was used with a real-space cutoff at 11 Å, whereas a force-switched cutoff starting at 9 Å and ending at 10 Å was used for Lennard-Jones nonbonded interactions. The rigid-rod-dipole method for gold atom polarization was implemented as for the existing GolP FF.[33,34] Random initial dipole positions were used throughout.

To identify the minimum energy structure of each small molecule when adsorbed, short simulated annealing molecular dynamics (MD) simulations of up to 40 ps were carried out. The temperature of the gold dipoles was maintained at 300 K throughout, while that of the adsorbate was incrementally decreased to 1 K. At least five different annealing cycles were performed per adsorbate, starting from different initial adsorbate conformations.

Classical interaction energies were calculated following two 50 ps constant-temperature (300 K) MD simulations: the first with the molecule midway between the gold slab and its periodic image, and the second with the molecule adsorbed on the surface. During both, all atoms were kept fixed in their initial relaxed positions with only the gold dipoles able to freely rotate. The nonelectrostatic contribution to the interaction energy is the difference between the bond, angle, dihedral, and LJ components of the potential energy of the bound and free molecule systems. The *free* energy of the electrostatic interaction between the adsorbed molecule and the ensemble of dipoles (F_{Coul}) was approximated from the difference between the average electrostatic energies (E_{Coul}) using eq 4, which has been derived previously.[34]

$$F_{\text{Coul}} = \frac{E_{\text{Coul}}}{2} \quad (4)$$

MD SIMULATIONS

Aqueous Au(111)/Au(100) Interface. MD simulations of the aqueous Au(111) and Au(100) interfaces were performed to investigate facet-selective differences in water structuring above each surface, using the newly derived FF parameters. Gold slabs, of dimensions 43.95×40.60 Å^2/29.30×29.30 Å^2 ((111)/(100)) were solvated with 2040/1425 modified TIP3P[74,75] water molecules. Newton's equations of motion were solved using the Leapfrog algorithm,[76] with a time step of 1 fs. Simulations, of duration 5 ns, were conducted in the *NVT* ensemble, with frames saved every 1 ps; the Nosé–Hoover thermostat was used to maintain the temperature at 300 K, while the cell dimension in the direction normal to the surface was adjusted prior to the simulation to give bulk water density for TIP3P waters under the same conditions midway between opposite gold facets. PME electrostatic summation was cutoff at 13 Å, and a force-switched cutoff starting at 10 Å and ending at 11 Å was used for Lennard-Jones nonbonded interactions.

Amino Acid Adsorption. The adsorption of five amino acids (Ala, Arg, Asp, His, Lys) onto Au(111) under aqueous conditions has been investigated by means of MD simulation using conditions as specified above. Amino acid termini were capped by acetyl/N-methyl groups (N/C-termini, respectively) to allow qualitative comparison with peptide binding experi-

ments.[58] The protonation state of residue side-chain functional groups at pH 7 has been modeled, with a counterion (either Cl^- or Na^+) added to achieve overall cell neutrality where required. Both protonated (HisH) and unprotonated (HisA) forms of histidine have been modeled.

To calculate the potential energy change of adsorption, a "compartmentalized" approach has been adopted.[26,77,78] Following the protocol of Heinz,[78] 10 independent simulations were carried out for each amino acid: half of the capped amino acid at the aqueous Au(111) interface and half of the capped amino acid in solution. Amino acid gold simulations were all initiated with the adsorbate positioned close to the interface (typically with an amino acid center-of-mass (c.o.m)−gold distance of 3.7 to 5.3 Å, depending on initial conformation and size of the amino acid) and were of 10 ns duration. Ten further simulations, five of the aqueous gold interface and five of water only (each 5 ns long), were carried out. Simulations of the amino acid in solution were also run for 5 ns. All cells contained a total of 2040 TIP3P water molecules. Amino acid gold conformations were first relaxed during a 1 ns simulation in which the separation between the c.o.m of the amino acid and the gold surface was restrained using a weak harmonic spring (force constant 500 kJ mol^{-1} nm^{-2}) to minimize unfavorable surface contacts without desorbing the molecule. Multiple starting configurations, differing in initial amino acid (and amino acid gold) conformation, have been used to ensure adequate sampling of phase space without the need for lengthy individual simulations.

In order to calculate the potential energy of adsorption, volume was conserved between each of the four "compartments" used in the calculation.[78] The lateral dimensions of all cells were kept constant with only the z dimension varied. Short simulations in the *NPT* ensemble were carried out for the solvated amino acid and water-only systems to determine the equilibrium volume at a pressure of 1 bar. The volume of the water/gold and amino acid/gold cells was then adjusted using a series of short *NVT* simulations to determine the z dimension for which the density of water midway between the upper and lower surfaces of the slab was the same as that of bulk water in the solution based cells.

Analysis. The structure of interfacial water at the Au(111) and Au(100) interfaces was analyzed using data from the final 2 ns of each trajectory. The mass density profile of water was calculated above each surface. The thickness of the first adsorbed water layer was defined as the difference between the z coordinate of the most exposed gold atom in the surface and the position of the first minimum in the water density profile. Hydrogen bonds were defined using the criteria of Cicero et al.,[79] namely an O···O distance of less than 3.5 Å and an O···HO angle greater than 140°. Data for the in-plane distribution of water molecules within the first adsorbed layer, and the orientation of water molecules as a function of distance from the gold surface, and the procedure used to calculate them are given in the Supporting Information.

As a qualitative probe of surface hydrophilicity, the adsorption of a water droplet, comprising 1000 TIP3P molecules, onto the Au(111) and Au(100) surfaces was also simulated. Extended gold slabs of surface areas 131.9 × 121.8 $Å^2$ and 146.5 × 146.5 $Å^2$ were used for the Au(111) and Au(100) facets, respectively, while the cell dimension in the direction normal to the surface was 120.0 Å in both cases. Simulations were carried out until the characteristics of the water droplet had converged (3−4 ns).

The change in potential energy of a system on the adsorption of an adsorbate, ΔE_{ads}, can be used to approximate the binding affinity of the molecule; if the entropic change is negligible, then this is a good approximation to the binding free energy. Here, we have determined ΔE_{ads} of each capped amino acid by the difference in potential energies of surface and solution simulations[21,26,77,78] using the following method:

$$\Delta E_{ads} = E_{tot} - E_{aw} - E_{wg} + E_{w} \quad (5)$$

where ΔE_{ads} is the potential energy change of adsorption; E_{tot} is the average potential energy of the solvated, capped amino acid gold system; and E_{aw}, E_{wg}, and E_{w} are the average potential energies of the solvated amino acid, water−gold, and water-only systems, respectively. The final 4 ns of each of the five simulations was used to calculate the average potential energy of the system, $E_{sys,i}$ (sys = tot, aw, wg, w), where i = 1−5 is the simulation number; E_{sys} and σ_{sys}, the mean and standard deviation from the mean, were then calculated using data from the five independent simulations with identical composition. The errors in each component of ΔE_{ads}, σ_{sys}, were propagated in the normal manner to give σ_{ads}. Finally, the role of entropy in amino acid gold binding was explored using the original GolP FF,[33] for which free energy of adsorption data exist[27] (see SI section GolP: Amino-acid Potential Energy of Adsorption Calculations for more details).

To further probe amino acid binding propensity, the c.o.m-surface separation of the entire capped amino acid was monitored during each of the five surface-bound trajectories. Favorable amino acid/gold conformations have also been identified by monitoring the binding propensity of the key functional groups (capped N/C-termini and side-chain) over the final 4 ns. A functional group was defined as "bound" when its c.o.m. was within 4 Å of the surface.

RESULTS AND DISCUSSION

vdW-DFT Adsorption Energies on Au(111) for Small Molecules in Vacuo: Comparison with Experiments. In recent years the vdW-DF functional has been successfully applied to a number of different systems,[63,64,80] including small molecule-Au(111) adsorption.[69,81−83] However, these studies have been limited to aromatic adsorbates and have employed revPBE[65] and PBE[71] functionals. In addition, while it has been shown that vdW-DF can accurately reproduce van der Waals interactions at minimum energy separations, a number of limitations have also been identified:[84] (1) equilibrium separations can be overestimated, (2) dispersion interactions can be overestimated at intermediate separations, and (3) hydrogen-bond strengths can be underestimated. In light of these factors, it was necessary to evaluate the suitability of using vdW-DF/revPBE to investigate the adsorption of small molecules on gold for a number of different functional groups. We accomplished this by comparing the experimental[85−89] and calculated interaction energies of a range of adsorbates on Au(111).

Our data show that vdw-DF is able to reproduce experimentally determined interaction energies for small-molecule gold adsorption (Figure 2). The slight tendency for PW-DFT interaction energies of unbranched molecules of long aspect ratio to be larger than the experimentally reported values is consistent with a recent molecular simulation study.[90] Specifically, Fichthorn et al. found that the pre-exponential factor used in the method to calculate alkane interaction

energies from raw experimental data increased with chain length, a fact that had not been accounted for.[85] As a result, the experimental interaction energy of dodecane with Au(111) was thought to be underestimated by as much as 24 kJ mol^{-1}.[90] Taking this into account, we believe that vdW-DF is a reliable, computationally accessible first-principles method that accounts for dispersion, appropriate for use in the small molecule−gold interaction energy calculations necessary to derive FF parameters.

Au(111). Following the GolP methodology, and for reasons outlined in the Methods, we have introduced virtual interaction sites into the surface topology to enable the FF to reproduce the favorable geometries of small molecules relative to the underlying gold surface identified by the vdW-DF calculations. For the Au(111) surface there are two virtual sites (denoted AUI) for every real gold surface atom (denoted AUS), located in the two hollow sites of each surface unit cell (Figure 3a). It was shown previously that the same LJ σ_{Au-Au} and ε_{Au-Au} parameters can be applied to both virtual sites and gold atoms within the bulk (denoted AUB) without loss of accuracy.[33] The spatial extent of gold atoms in the surface is described indirectly via the virtual interaction sites only, with no LJ terms being assigned to AUS.

It is important to stress that in the work presented here, both the energy and geometry of the adsorbed molecules have been used to refine the FF, as both properties could be important in determining biomolecule facet selectivity. However, several groups have shown that vdW-DF overestimates the equilibrium separation between two molecules[62,63,84] or between a molecule and a surface.[81,84,91] Therefore, it was not appropriate to fit FF parameters to match these calculated distances exactly. After reviewing the literature, we have adopted a tolerance of ∼0.2−0.3 Å when parametrizing the FF; the FF still predicts the *trend* in equilibrium separations from the Au(111) and Au(100) surfaces correctly, relative to vdW-DF calculations. For the Au(111) facet, experimental energetic data have been used in the fitting process, where available.

GolP-CHARMM parameters for the Au(111) surface are presented in Table 2. The quality with which the FF fits both reference and test set data and the choice of parameters for this surface are discussed herein; for further details, see Figure 4 and Figures S2 and S3 and Tables S1, S2, and S3 in the Supporting Information.

Table 2. GolP-CHARMM LJ Parameters for the Au(111) Surface[a]

	AUI		AUB	
	ε, kJ mol^{-1}	σ, Å	ε, kJ mol^{-1}	σ, Å
Au−Au	0.48	3.80	0.48	3.80
Au−Au (π-C)	1.30	3.20	0.48	3.80
Au−N (imidazole)	1.60	2.85	1.60	2.85
Au−N (unprotonated N termini)	0.90	2.90	0.90	2.90
Au−S	3.20	2.85	3.20	2.85
Au−O	0.70	3.10	0.70	3.10
Au−H	0.28	2.70	0.28	2.70

[a]Interaction strengths ε (kJ mol^{-1}) and distances σ (Å) are given for both surface virtual sites (AUI) and bulk gold atoms (AUB). Note the Au−H interaction is for hydroxyl and amide H only.

Using the generic Au−Au LJ parameters (to be combined with all CHARMM atom types other than the special cases described below), the root mean squared deviation (RMSD) between experimental[85] and GolP-CHARMM interaction energies for alkane adsorption was 1.88 kJ mol^{-1} (Figure S2). The marked difference between these GolP-CHARMM parameters and those used in the existing GolP FF is a direct consequence of both energetic and spatial data being used in the fitting procedure. In fact, choosing LJ parameters for GolP-CHARMM that are closer to the OPLS-AA values (σ_{Au-Au} = 3.2 Å, ε_{Au-Au} = 0.75 kJ mol^{-1} GolP-CHARMM; σ_{Au-Au} = 3.2 Å, ε_{Au-Au} = 0.65 kJ mol^{-1} OPLS-AA) also gave a reasonably good fit to the adsorption energy for alkanes (RMSD = 2.92 kJ mol^{-1}) but resulted in adsorption geometries for which the molecules were too close to the surface.

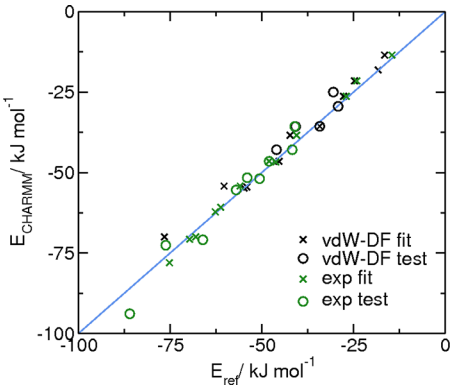

Figure 4. Comparison between the interaction energies of small molecules with Au(111) *in vacuo* calculated using GolP-CHARMM FF and either experimental data (green) or those calculated using the vdW-DF exchange functional (black). Both molecules used to derive FF parameters (crosses) and those in the test set (open circles) are shown. The solid blue line denotes 1:1 correlation.

Following the procedures originally developed with GolP,[33] a different set of Au−Au LJ parameters was developed to refine the nonbonded interaction between gold and sp^2 hybridized carbon atoms within carbon−carbon multiple bonds (e.g., aromatic rings and isolated or conjugated C═C bonds). In the absence of these customized terms, the affinities of ethene,[85] benzene,[85,92] and 1,3-butadiene[85] for the Au(111) surface were underestimated to a similar degree in GolP-CHARMM to that reported previously for OPLS-AA.[33]

Sulfur-containing moieties and functional groups featuring a nitrogen atom with a lone pair of electrons were shown previously to chemisorb weakly onto the Au(111) facet.[33] PW-DFT calculations, performed here using vdW-DF, confirmed these findings. It was not possible to represent this weak chemisorption using standard mixing rules to combine CHARMM potentials with the generic Au−Au potential described so far: the resulting FF substantially overestimated the binding distance and underestimated the energy of interaction. We have therefore introduced specific LJ cross-terms for the Au−S (fitted to methanethiol and methyl sulfide adsorption) and Au−N interactions. Indeed, for nitrogen we also found it essential to differentiate between N atom types in aliphatic and aromatic groups when fitting these special interaction parameters—a consequence of the different electron density distributions surrounding N atoms in these environments polarizing the gold surface by dissimilar amounts and bringing about differences in overlap and dispersion forces between the N atom and the surface. We have therefore fitted separate Au−N cross-terms for unprotonated histidine residues

dx.doi.org/10.1021/ct301018m | J. Chem. Theory Comput. 2013, 9, 1616−1630

(to reproduce imidazole−Au(111) adsorption) and for unprotonated amino acid/peptide N-terminal groups and lysine residues. This second set was fitted to methylamine−Au(111) adsorption. Methylamine, featuring an alkyl group, is a better analogue of the unprotonated N-terminus than ammonia, originally used in GolP. Since polar hydrogens bonded to N already have a small spatial extent in CHARMM, unlike OPLS-AA, no additional Au−H(N) parameters for the *amine* H atoms were required.

The issues with the heteroatoms N and S also extended to organic oxygen. In particular, using the terms described above, the FF is able to reproduce the correct interaction energy for methylamide adsorbed onto the Au(111) surface but gives the wrong geometry as the Au−O interaction is too weak in comparison to the Au−N. In fact, the affinity of all oxygen containing moieties to Au(111) was consistently underestimated. We have therefore extended the FF to include a specific Au−O cross-term as well. It is important to note that for GolP-CHARMM to correctly describe both the binding energy and geometry of amide group adsorption onto Au(111), a new atom type must be introduced into CHARMM to differentiate between an amide and unprotonated amine N. The refined Au−N cross terms should be applied only to the interaction of the former, the unprotonated *amine* nitrogen atoms, with gold.

In reparametrizing the Au(111) surface to be compatible with CHARMM, we have addressed a specific aspect of the description of the Au(111)−liquid water interface that remains unresolved in existing classical FFs. CPMD simulations using the PBE functional (without van der Waals corrections) revealed that interfacial water molecules have an enhanced tendency to act as hydrogen bond donors to other water molecules, relative to those molecules in bulk liquid water.[79] This behavior is not captured by the original GolP/SPC and CVFF-METAL/SPC models.[79] A correction for GolP/SPC (i.e., to add a small Au−H(O) LJ interaction) was identified by Cicero et al.[79] Here, to reproduce the first-principles behavior using GolP-CHARMM, it was critical to ensure that the vdW-DF energetics and geometry of a single water molecule adsorbed onto Au(111) in vacuum could be reproduced. When using the generic GolP-CHARMM Au−Au LJ terms in combination with water atoms, O and H, not only was the affinity of a TIP3P water molecule for Au(111) significantly underestimated (−13.4 kJ mol^{-1} GolP-CHARMM vs −18.3 kJ mol^{-1} vdW-DF) but it was also mis-oriented with one of its H atoms pointing toward the gold surface (Figure 5a). Configurations similar to this were sometimes found for SPC waters at the (uncorrected) GolP Au(111)−water interface.[79] This orientation hinders the molecule from acting as a hydrogen bond donor to surrounding waters. In the current work, we found it necessary both to increase the strength of the interaction between the water oxygen atom and the gold surface and enlarge the spatial extent of its hydrogen atoms. While it was not possible to make the preferred TIP3P−Au(111) conformation identical to that found in vdW-DF calculations (Figure 5b), the optimal configuration for a single water molecule adsorbed at the interface (Figure 5c) at least does not impair its potential to act as a hydrogen bond donor when surrounded by liquid water.

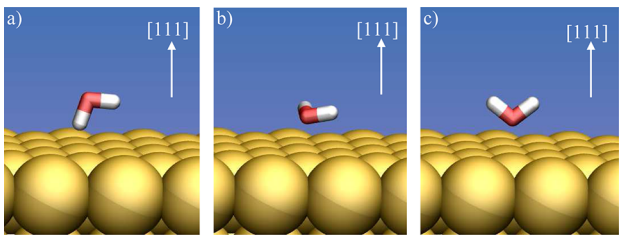

Figure 5. The most favorable orientation of a single water molecule adsorbed onto Au(111) (a) using the FF without extra Au−O LJ parameters, (b) using vdW-DF, and (c) using the new FF with Au−O LJ parameters.

Au−O and Au−H LJ cross parameters that were fitted to water adsorption were found subsequently to be transferable to other small molecules. Only for methanol is the affinity for gold still underestimated by the FF, although this discrepancy was reduced from 8.7 kJ mol^{-1} to 5.5 kJ mol^{-1} by the inclusion of Au−O and Au−H parameters.

As an initial validation of the FF we calculated the *in vacuo* binding energy of a number of small molecules that had not been used in the fitting process on Au(111), for comparison with experimental data[85,86,89] (Table S2). The test set was chosen to benchmark the interaction of a range of different functional groups, both independently and in combination, with Au(111). For example, the transferability of the generic Au−Au LJ parameters derived using linear alkanes to cyclic systems was tested with cyclohexane, while the ability of the new FF to describe the adsorption of a molecule with more than one independently parametrized functional group was tested with non-1-ene, trans-2-butene, ethanethiol, dibutyl sulfide, and toluene. The agreement between GolP-CHARMM and experimental data was comparable to that of GolP (RMSD of interaction energy of 4.15 kJ mol^{-1} for GolP-CHARMM; cf. 4.97 kJ mol^{-1} for GolP[33] for a similar set of test molecules, see Table S2 for details).

Ideally, FF parameters for all of the functional groups present in a peptide would be benchmarked against experimental results obtained in a consistent manner, but such data are not available. Therefore we have tested the transferability of the Au−O and Au−H parameters, which were not probed by the experimental test set (Table S2) using vdW-DF calculations (Table S3). However, for charged molecules, we found from extensive calculations that the PW-DFT interaction energies depended on the simulation cell dimensions—far more strongly than would be expected for electrostatic interactions alone[93]—and so cannot be used reliably to determine the binding affinity to gold *in vacuo*. NH_3^+ and COO^- moieties, in particular, are prevalent in biomolecules, being featured by all uncapped peptide termini under neutral pH conditions. Hence it is essential to be sure that our new FF parameters are also transferable to these groups for meaningful biointerfacial-gold simulations. To do this, we have included positively and negatively charged amino acids (Asp, Arg, Lys) in the test set of five amino acids that we have simulated at the aqueous Au(111) interface using MD and compared trends in the potential energy of adsorption to those observed experimentally[58] (see subsection Amino Acid Adsorption).

Au(100). A procedure consistent with that used to parametrize Au(111) was employed to derive FF parameters for Au(100), as summarized in Table 3. In this case, all reference small-molecule interaction energies used in the fitting were obtained from vdW-DF calculations, as appropriate experimental data are not available for this surface. As with Au(111), it was again necessary to assign LJ parameters to virtual interaction sites on the surface rather than associate

Table 3. GolP-CHARMM LJ Parameters for the Au(100) Surface[a]

	AUI		AUB	
	ε, kJ mol^{-1}	σ, Å	ε, kJ mol^{-1}	σ, Å
Au−Au	2.10	4.00	2.10	4.00
Au−Au (aromatic C)	2.80	3.40	2.10	4.00
Au−N (imidazole)	4.40	3.00	4.40	3.00
Au−N (unprotonated N termini)	5.40	3.00	5.40	3.00
Au−S (sulfide)	6.90	3.00	6.90	3.00
Au−S (thiol)	5.20	3.00	5.20	3.00
Au−O(= C)(carbonyl)	0.60	3.35	0.60	3.35
Au−O(−H)(water/methanol)	1.50	3.275	1.50	3.275
Au−H	0.60	2.725	0.60	2.725

[a]Interaction strengths ε (kJ mol^{-1}) and distances σ (Å) are given for both surface virtual sites (AUI) and bulk gold atoms (AUB). Note the Au−H interaction is for hydroxyl, amide, and thiol H only.

them directly with the gold surface atoms (Figure 3b, see Figure S1 in the Supporting Information for more information about the alternative schemes tested). Employing a scheme with virtual sites located in the hollow sites of the surface is, on one level, consistent with Au(111). However, differences in surface structure mean that the density of hollow (virtual) sites on Au(100) is less than half that on Au(111). As a consequence, FF parameters are not transferable between the two interfaces and are, in some cases, of a different order of magnitude.

A similar set of small molecules was chosen to parametrize the Au(100) surface (Table S4) to that used for Au(111). Generic Au−Au LJ parameters, for use with all CHARMM atom types other than those individually parametrized below, were fitted to the interaction energies of methane and butane; hydrocarbon chains of longer lengths are not present in peptides and so were not considered in our fitting procedure. As with Au(111), it was necessary to define a number of other distinct gold−organic cross-terms. Following our earlier protocol, we have derived a refined Au−Au potential for sp^2 hybridized carbon atoms present in carbon−carbon multiple bonds, and specific cross-terms for heteroatom−gold interactions (S, N, and O). However, for this interface, we found that the transferability of these cross-terms was less effective than for the Au(111) surface.

This is best exemplified by the adsorption of hydrocarbon molecules with sp^2 hybridized carbon atoms on Au(100) *in vacuo*. Using only generic Au−Au LJ parameters, the affinities of benzene and ethene for Au(100), relative to vdW-DF, were underestimated by 7% and 31%, respectively, although the resulting geometries were consistent with those obtained from PW-DFT calculations; in particular, the mid point of the ethene C═C bond was located atop a Au surface atom, and the center of the benzene ring was commensurate with a hollow site (Figure S4). Therefore, as with the Au(111) surface, in order to more accurately describe the adsorption of these molecules, it was necessary to derive a refined set of Au−Au LJ parameters to use in combination with this subset of CHARMM carbon atom types. However, for Au(100) it was not possible to derive a single set of customized Au−Au LJ terms to be combined with sp^2 hybridized C atoms that was transferable between different chemical environments (e.g., aromatic rings, isolated C═C and conjugated C═C bonds). The computational expense of the PW-DFT calculations necessary to derive and test modified Au−Au parameters for different types of C═C bonds (isolated and conjugated) was beyond the scope of this work (to present a FF for *peptide*−gold adsorption, where isolated C═C bonds are not present) and has not been carried out. As a repercussion, only one set of customized Au−Au parameters is presented in Table 3. These parameters, fitted to benzene adsorption, transferred well, both in terms of energetics and adsorbate-gold conformation, to the other small molecules containing aromatic rings, e.g., phenol, indole, and toluene (Table S5)

A greater dispersity of interaction is also seen with heteroatoms on the Au(100) surface. In particular, thiols and dialkyl sulfides were found to interact quite differently from each other with the Au(100) surface and required different Au−S cross-terms to be defined for the two cases. These were parametrized with methanethiol and dimethyl sulfide, respectively. In practical terms, this requires a new atom type to be introduced into CHARMM in order to differentiate between the two S atom environments, though we note that the organic interactions associated with these two S atom types are identical. In addition, the σ parameter for the Au−H(S) interactions must be increased to prevent them from approaching the Au(100) interface too closely. This is in contrast to Au(111) and arises from the lower surface density of virtual sites on the Au(100) surface.

As with the Au(111) interface, vdW-DF calculations revealed that ammonia, imidazole, and methylamine are all weakly chemisorbed to Au(100). Again two sets of Au−N parameters are needed to reproduce the correct adsorption of both types of unprotonated N. For consistency between the two surfaces, methylamine was used to fit Au−N parameters for unprotonated amine-gold binding, while imidazole was used to fit Au−N parameters for an unprotonated N atom in aromatic groups, such as the side chain of histidine. As with the Au(111) interface, the former set of parameters is not transferable to *amide* N, and so, as before, introduction of a new atom type is necessary in CHARMM.

As with all biointerfacial FFs designed to be used in aqueous conditions, parameters that adequately describe the structure of liquid water above Au(100) are essential. Here, we have derived parameters in a manner consistent with the Au(111) FF, namely fitting Au−O and Au−H cross-terms to the energetics and adsorption geometry of a single water molecule adsorbed onto the Au(100) surface, as determined from PW-DFT calculations. Au−H parameters, identical to those used for thiol H, were chosen for consistency. However, in the absence of experimental or first principles MD data, validation is difficult. Specifically, there is no evidence to suggest what the favorable water−gold orientation would be for the gold−liquid water interface. We can only check our parameters here on the level of single water adsorption against PW-DFT calculations. Hence, we used a number of different initial water−gold adsorption geometries ("O down," "1H down," "2H down," and "flat") to probe adsorption onto each of the three main surface sites (bridge, hollow, top) in a variety of orientations.

Importantly, trends in the energetics of binding to the different surface sites (top, bridge, hollow) are captured by the FF, with adsorption atop a surface Au atom being the most favorable at both interfaces (Table 4). As was found for the Au(111) interface, water, when atop Au, is found by vdW-DF calculations to be preferentially oriented with its plane tilted with respect to the surface (with the angle between surface

Table 4. Interaction Energy of Water Adsorbed at Different Surface Environments on the Au(100) Surface (kJ mol^{-1}), Calculated Using vdW-DF and GolP-CHARMM

	E_{vdW-DF}	$E_{GolP-CHARMM}$
bridge	−17.7	−18.6
hollow	−15.1	−14.1
top	−20.8	−19.8

normal and water dipole moment being 62° for Au(100) and 68° for Au(111)), while using FF parameters it adopts an "O down" conformation. Although differences exist in these water−gold conformations, critically for biomolecule adsorption, as discussed above, both hydrogens are available to act as hydrogen bond donors. More profound deviations from vdW-DF in terms of the conformation of an adsorbed water molecule were only found when unfavorable adsorption sites were considered. For adsorption at both bridge and hollow sites, the most favorable water orientation found from vdW-DF calculations was "flat" and "O down," respectively, while for the FF it was "2H down." The difference in energy, calculated using vdW-DF, between "O-down" and "2H-down" configurations is only 3.0 kJ mol^{-1} and 1.0 kJ mol^{-1} for bridge and hollow sites, respectively. Such small energy differences, while influential at 0 K on the single molecule level, are expected to be less prominent in MD simulations carried out under ambient conditions. Hence, while the FF may not be able to reproduce accurately all the fine detail in the potential energy landscape for the adsorption of a single water molecule on the Au(100) surface that is evident in vdW-DF calculations, the FF is able to reproduce the key features.

Unlike the Au(111) interface, in the absence of specific Au−O parameters, only the binding affinities of water and methanol were underestimated relative to vdW-DF; the Au−O parameters fitted to water adsorption were valid for methanol. Therefore, this set of special Au−O cross-terms is only applicable to hydroxyl oxygen atoms attached to aliphatic carbon atoms or water. In CHARMM, the oxygen in aliphatic, aromatic, and acidic hydroxyl groups all share the same atom type. Hence, as with thiol and sulfide S, a new atom type must be introduced in order to differentiate between the different gold binding affinities of O in different hydroxyl environments. Au−H parameters, on the other hand, were transferable to the other polar hydrogen environments which share the same atom type as an alcohol H (e.g., an *amide* H).

While it was possible to reproduce the energetics of the carbonyl oxygen−gold interaction using the generic Au−Au LJ parameter set for this facet, the resulting geometries were not so good. In particular, the equilibrium separations of methanoic acid and methylamine from the Au(100) surface were greater than those at the Au(111) facet *in vacuo* using the new FFs, opposite to the trend observed for vdW-DF. Hence, a further set of Au−O LJ parameters, this time specific to carbonyl oxygens only, was fitted to reproduce the energetics and trends in spatial facet selectivity of methyl amide adsorption. These parameters transferred well to methanoic acid.

As an initial test of the Au(100) FF parameters, we calculated the interaction energies of seven small molecules (methanol, indole, methanoic acid, phenol, ethanethiol, diethyl sulfide, toluene) that had not been used in the fitting procedure and compared the FF predictions with the results of the PW-DFT calculations (Table S5). Most of the different functional groups parametrized above are represented by this group, either independently or in combination. In addition, the adsorption of side-chain analogues of all 20 amino acids onto Au(100) was studied using both the new FF and PW-DFT. The agreement between FF and vdW-DF interaction energies for the test set was good, with an RMSD in the interaction energies of 3.64 kJ mol^{-1} (Figure 6). The largest outlier was ethanthiol, where the strength of Au(100) binding was overestimated by approximately 12%.

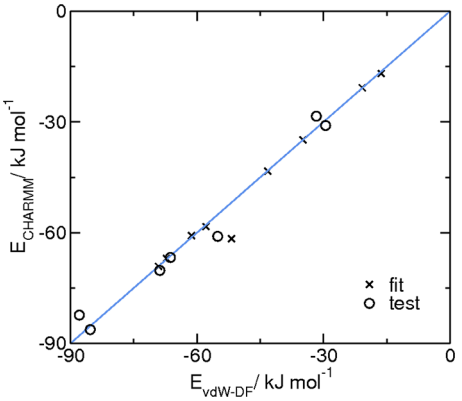

Figure 6. Comparison between the interaction energies of small molecules with Au(100) *in vacuo* calculated using GolP-CHARMM to those calculated using the vdW-DF exchange functional. Both molecules used to derive FF parameters (crosses) and those in the test set (open circles) are shown. The solid blue line denotes 1:1 correlation.

FACET SELECTIVITY OF SINGLE MOLECULE ADSORPTION

The first-principles calculations required to derive GolP-CHARMM parameters also offer a unique insight into the facet selectivity of small molecule−gold adsorption *in vacuo* on a single molecule level (Figure 7, left); to date no such systematic study has been carried out. Energetically, the strength of adsorption onto either of the two facets studied, Au(111) or Au(100), is comparable. Selectivity is greatest among those molecules displaying weak-gold chemisorption, with affinity for the Au(100) facet being stronger (Figure 7a, left). Spatially, optimal adsorbate−gold conformations on each facet are also similar, with heteroatom and C═C bond adsorption preferentially being atop Au surface atoms and the centers of aromatic rings lying above hollow sites (Figures S3 and S4). In correlation with energetic data, equilibrium adsorbate−gold separations are smaller for the Au(100) facet (Figure 7b, left).

The trend in facet selectivity of amino acid analogue gold binding observed from PW-DFT calculations *in vacuo* is different from that obtained previously by classical MD in water[19] where adsorption onto Au(111) was found to be more favorable than that onto Au(100). It is highly likely that the difference is due to the presence of water. The binding affinity of a single water molecule for the Au(100) surface is approximately 14% stronger than that for Au(111), meaning the strength of biomolecule−gold adsorption *relative to that of liquid water* may yet be weaker at the former interface.

Only extensive simulations and rigorous experiments, under clean and well-defined conditions, probing the adsorption of all amino acids or short peptide sequences onto different gold surfaces under aqueous conditions, can allow firm conclusions

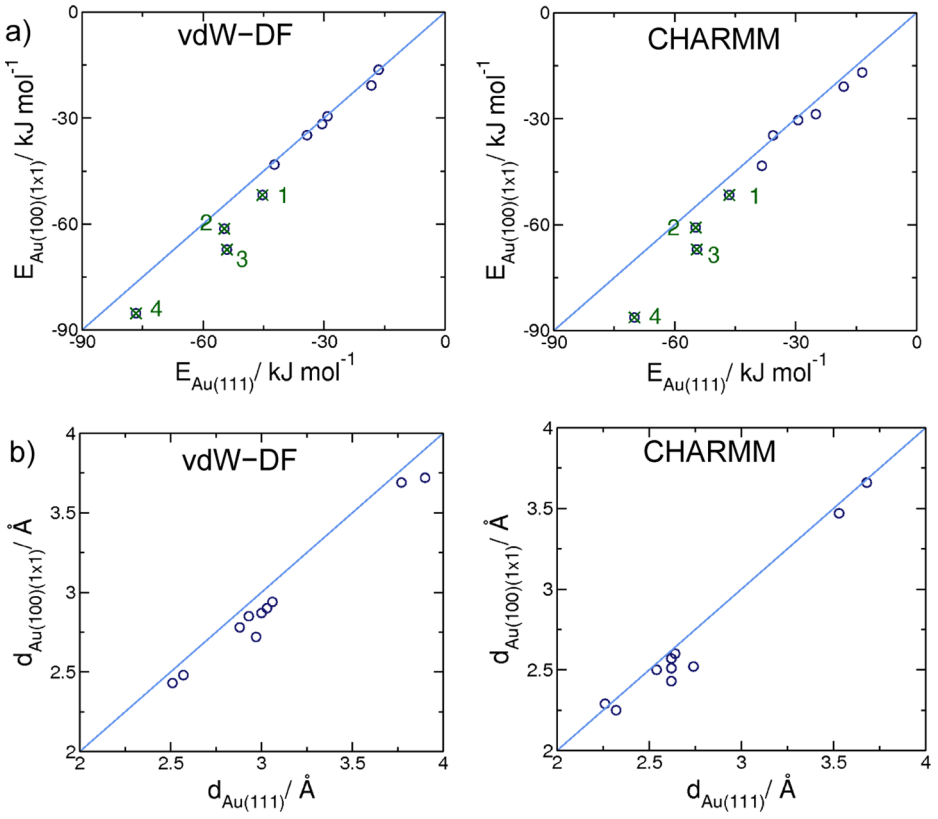

Figure 7. (a) Energetic and (b) spatial facet selectivity of small molecule adsorption onto Au(111) and Au(100) *in vacuo* obtained from vdW-DF (left) and GolP-CHARMM (right) calculations. GolP-CHARMM data shown only for those molecules for which vdW-DF calculations have also been carried out. Molecules observed to weakly chemisorb onto gold (1, methanethiol; 2, methylamine; 3, imidazole; and 4, diethyl sulfide) have been highlighted in (a).

to be drawn about facet selectivity of biomolecule−gold adsorption. However, the FFs parametrized here can capture the same trends in facet selectivity of small molecule adsorption *in vacuo*, both spatially and energetically, as those observed using PW-DFT (Figure 7, S5), and so we believe GolP-CHARMM to be an acceptable alternative, able to access the time and length scales necessary for such a comprehensive study.

Aqueous Au(111) and Au(100) Interfaces. It is essential for future biointerfacial simulations that the new FFs can model liquid water at both the Au(111) and Au(100) surfaces, since it has been previously shown that water structuring above an inorganic surface can strongly influence biomolecule adsorption.[94−96] However, few unambiguous *atomistic* descriptions of *liquid* water adsorbed onto gold exist. Only the *aqueous* Au(111) interface has been previously studied at the first-principles level of theory,[79,97] although several groups have used Born−Oppenheimer MD (BOMD) to probe water bilayer adsorption onto both Au(111)[98,99] and Au(100)[100] *in vacuo*.

A review of the literature and further calculations carried out here show that the conformation of a single water adsorbed onto the Au(111) facet *in vacuo* is only marginally dependent on the exchange functional employed,[97] with PBE,[79] PBE-D,[79] PW91,[98] vdW-DF, and BLYP all favoring O atop Au atom geometries. Although this consensus at the single molecule level is not sufficient to prove the same for liquid water, we have chosen to benchmark the Au(111) FF parameters for water adsorption against the CPMD study of Cicero et al.[79] despite long-range dispersion interactions not being accounted for in this work. Very recently, Nadler and Sanz performed BOMD simulations on the Au(111)−water interface.[97] They used the PBE,[71] PBE-D2,[101] and optB86b-vdW[102] functionals and obtained results in qualitative agreement with the work of Cicero et al.[79] Hence, the absence of dispersion should not stop the CPMD simulations from being a suitable benchmark for GolP-CHARMM.

Our new FF gave good overall agreement with the structure of water above Au(111) exhibited during CPMD simulations (Figure 8). The new FF reproduced the enhanced tendency of interfacial water molecules to act as hydrogen bond donors compared with those in bulk liquid water (Figure 8b). The ability of the FF to capture these subtle water characteristics is critical for improving the accuracy of biointerfacial simulations, where hydrogen bonding to first-layer adsorbed waters may enhance or facilitate biomolecule-surface binding.[96]

Detailed analysis of water−gold conformation as a function of surface separation reveals that, for the Au(111) surface, molecules in the first layer are oriented in an ordered fashion, with a preference for the oxygen atom in a water molecule to lie closer to the interface than the hydrogen atoms (Figure S6). The modal angle between the dipole moment of these waters and the surface normal was 90°, however, similar to the geometry of a single water adsorbed *in vacuo* onto the same surface calculated using vdW-DF (Figure 5b). Conformations such as this were also observed to be favorable for the subset of molecules residing in the first adsorbed layer in the CPMD simulations and which gave rise to a shoulder in the mass density profile close to the gold surface.[79]

GolP-CHARMM shows improvement in its description of the Au(111)−water interface over both the original GolP and

dx.doi.org/10.1021/ct301018m | *J. Chem. Theory Comput.* 2013, 9, 1616−1630

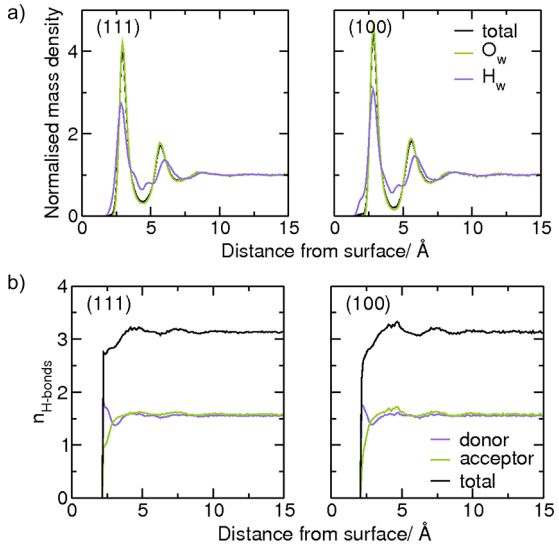

Figure 8. (a) Mass density and (b) the number of hydrogen bonds formed by waters as a function of surface separation from the Au(111) and Au(100) interfaces.

the CVFF/SFC FFs. Unlike GolP, GolP-CHARMM does not require any further corrections[79] to be able to reproduce the predominance of water molecules acting as hydrogen bond donors at the interface. While at odds with CVFF/SFC, it correctly reproduces the preference of water for top site adsorption. In addition, only GolP-CHARMM has been specifically fit to reproduce the energetics of single water molecule adsorption onto the Au(111) surface to PW-DFT data. It worth noting that if direct comparison is made between GolP-CHARMM and its predecessor, GolP,[33] then subtle changes in the structure and affinity of water at the aqueous Au(111) interface, brought about by the additional Au−O and Au−H(O) terms in GolP-CHARMM, may impact biomolecule adsorption. For instance, the interaction energy of a single water molecule *in vacuo* for Au(111) was −14 kJ mol^{-1} using GolP[33] but −18.1 kJ mol^{-1} using GolP-CHARMM. Thus, the competition between biomolecule and water adsorption on the gold surface is predicted to be less enthalpically favorable with GolP-CHARMM than with the original GolP. However, at the same time, the denser, more structured first adsorbed water layer featured by GolP-CHARMM means that the entropy change brought about by displacement of these waters into solution by an adsorbate would be larger. These two effects may partially cancel each other out.

Some discrepancies between GolP-CHARMM and the CPMD simulation of Cicero et al.[79] remain, however. First, using the FF, only a single population of water molecules in the first layer exists, with no shoulder on the O_w mass density profile in the direction normal to the surface. Therefore, the population of flat molecules (which dominate the shoulder observed in the CPMD mass density profile) and that of H-down molecules (dominating the rest of the first adsorbed layer in the CPMD simulation)[79] are less spatially segregated in GolP-CHARMM than in CPMD. Second, interfacial water remains relatively overstructured, with the density of the first adsorbed layer being greater using GolP-CHARMM than that found using first-principles forces. Despite these small differences, we believe that GolP-CHARMM can acceptably describe the aqueous Au(111)−gold interface.

The careful derivation of FF parameters for the Au(111) and Au(100) surfaces in a consistent manner allows detailed comparison between the structure liquid water above each interface for the first time (Figure, 8, S6, and S7). While for both surfaces there is a preference for interfacial waters to be oriented "O down" (Figure S6), facilitating their enhanced ability to act as hydrogen bond donors to surrounding water molecules (Figure 8b), this preference is marginally weaker in the case of Au(100). For instance, there is a small shoulder on the H_w mass density profile close to the interface for Au(100) only. Closer examination reveals that, in accordance with first layer water adsorption as a whole (Figure S7), the small subset of water molecules, oriented "H down," is preferentially adsorbed above top Au surface sites. In fact, for the Au(100) interface, the first layer water density is significantly more localized to top sites than is the first water layer on Au(111) (Figure S7). To check that this was not just a feature of the virtual site scheme employed for the former interface, simulations were also carried out using the scheme shown in Figure S1d. Similar results were obtained, with top sites being significantly more populated than the rest of the surface.

The density of the first adsorbed water layer normal to the surface was greater for Au(100) than Au(111) (4.4 × 10^3 kg m^{-3}, compared to 4.0 × 10^3 kg m^{-3}, Figure 8a), revealing that small differences in the energetic binding affinity of a single molecule *in vacuo* for each facet (2.8 kJ mol^{-1}) are translated into significant differences under *aqueous* conditions. However, both facets were observed to be extremely hydrophilic, in good agreement with experimental data;[103] a droplet of water was observed to spread to monolayer thickness within less than 200 ps upon adsorption.

The most pronounced differences in liquid water above the two gold surfaces, Au(111) and Au(100), are therefore the lateral arrangement and surface binding affinity, rather than the orientation of individual water molecules relative to gold. Only further simulations involving a variety of different biomolecules, with functionalities ranging from hydrophobic to hydrophilic, will reveal how this difference in the lateral arrangement of liquid water density at the interface will impact on facet selectivity of biomolecule adsorption.

Amino Acid Adsorption. To further test GolP-CHARMM for modeling polypeptide−gold adsorption under *aqueous* conditions, five capped amino acids adsorbed at the aqueous Au(111) interface have been simulated and the results compared to existing experimental[58,104,105] and computational data.[21,27−29] Within this test set, we have included amino acids with a range of side-chain functional groups, including positively, negatively, and uncharged species and those with planar aromatic rings and aliphatic carbon chains.

Out of the five amino acids tested, only alanine showed negligible energetic affinity to the aqueous Au(111) interface, while the strongest binding was exhibited by arginine and histidine (Figure 9); aspartate and lysine had intermediate affinity. These trends are in overall agreement with the experimental study of Cohavi et al.,[58] who recently determined the relative amount of free and BLIP (TEM1-β-lactamase inhibitor protein) fused homotripeptides bound to AuNPs and planar gold surfaces using Surface Plasmon Resonance (SPR) spectroscopy. In particular, the trend in binding strength of the free homotripeptides to AuNPs, 3His > 3Lys > 3Ala (and BLIP fused homotripeptides for continuous gold surfaces and discontinuous gold islands, 3His > 3Ala), is also seen with GolP-CHARMM. One notable difference between our

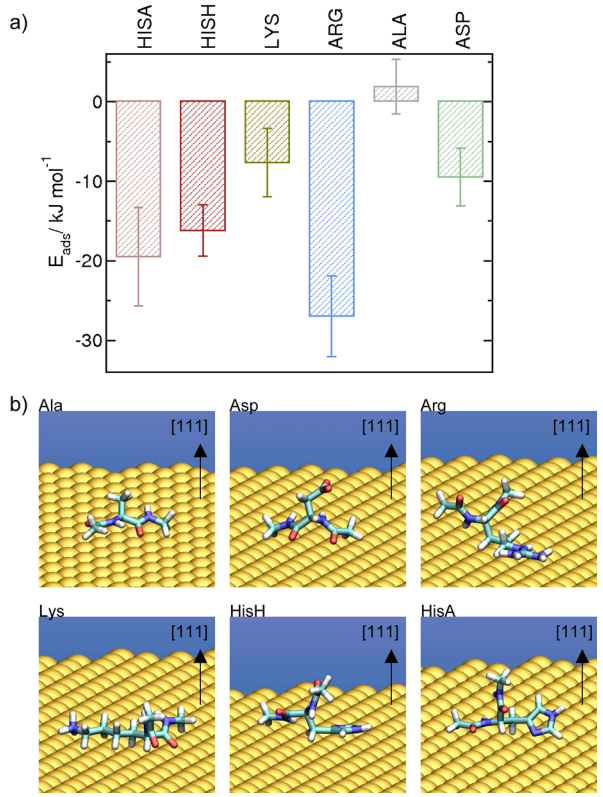

Figure 9. (a) Average potential energy change of adsorption for the capped amino acids histidine (protonated HisH, unprotonated HisA), lysine, arginine, alanine, and aspartate. (b) Snapshots of each amino acid adsorbed onto the Au(111) surface. Ala, depicted in a conformation in which both N and C termini are adsorbed; Asp, C- and N-termini adsorption; Arg, sidechain adsorption; Lys C-terminus and sidechain adsorption; HisH, side chain adsorption; and HisA, N-terminus and side chain adsorption. (Carbon atoms rendered in green, nitrogen in blue, oxygen in red, hydrogen in white, gold in orange. Water is not shown for clarity.)

calculations and the experimental results for BLIP-fused homotripeptide binding to AuNPs is the relative binding strength of Lys compared to Arg. With GolP-CHARMM, as with its predecessor GolP,[27,33] arginine binds to the Au(111) interface more strongly than lysine; the reverse is true of the BLIP-fused homotripeptides for AuNPs. However, the BLIP fusion proteins were observed to undergo structural changes and unfolding on adsorption,[58] suggesting that the relative amount of bound peptide measured in each case was a complex combination of the affinity between the 3X protein N-terminus and AuNP surface and tripeptide-BLIP-gold conformation. In addition, conformation of the homotripeptide itself could play a role, meaning that its binding affinity is not a simple multiple of that of its constituent amino acid.[23] In the case of arginine and lysine, it is possible that the more bulky nature of the guanidinium group relative to an alkyl ammonium moiety provides a greater steric hindrance to the coadsorption of all three residues in the respective homopeptides.

GolP-CHARMM also reproduces, qualitatively, the results of two earlier experimental studies. In the first, the relative binding affinities of interdigitated HXHXHXHX peptides for polycrystalline gold films[104] inferred from cell coverage assays identified the following binding affinities: His > Lys > Arg > Ala ~ Asp. Hnilova et al., on the other hand, used bioinformatics to determine the relative proportions of each amino acid in strong and weak binding gold peptides, relative to their overall expression in the FliTrx peptide library.[105] They reported Arg to be overexpressed in both weak and strong binders, while lysine and aspartate were under-expressed by strong binders and overexpressed by weak ones. Hence, while the work of Peelle et al. suggests that lysine has a stronger affinity for gold than arginine, in agreement with Cohavi et al.,[58] the results from the bioinformatics study are less conclusive. In addition, previous amino acid Au(111) adsorption MD studies using the two existing gold FFs, GolP[33] and CHARMM-METAL,[21] found arginine to have a greater affinity for the interface under aqueous conditions than lysine.[21,27,29] Therefore, although the experimental data necessary to validate GolP-CHARMM exhaustively are currently not available, we believe that our new FF is able to capture the physics and chemistry of the aqueous polypeptide-gold interface.

Alanine, which had no surface affinity, adopted an ambivalent conformation at the surface, with adsorption mediated by either or both capped termini and/or methyl side-chain all being equally likely (Figures 9b and S9). Amino acids Asp and Lys both had a tendency to adsorb to the surface via one capped terminus only (C-terminus in the case of Asp and N-terminus in the case of Lys). It is worth noting, however, that the cutoff used here to define the amino acid functional group, either a side-chain or capping terminus, adsorption was based on c.o.m.−surface separation and was the same for all amino acids, irrespective of side-chain size. Hence, although the lysine side chain was only infrequently "adsorbed" using this criterion, visual inspection of the trajectories reveals that it preferentially remains close to the interface, rather than protruding into liquid water. Experimental[58,104] and previous MD[21,27] studies all indicate that lysine has stronger binding affinity for Au(111) than aspartate, while the potential energies of adsorption for the two amino acids calculated here using GolP-CHARMM are, within error, identical. However, we hypothesize that differences in the entropic contribution to the free energy of adsorption (not accounted for in our calculations) between the two amino acids could be significant. This hypothesis is supported when the entropic contribution to the free energy of binding was estimated using the original GolP FF.[33] We found that for capped lysine $-T\Delta S_{ads} = -7 \pm 5$ kJ mol^{-1}, while for capped aspartate $-T\Delta S_{ads} = +2 \pm 5$ kJ mol^{-1} (Table S6, statistical errors are, however, significant). The more favorable entropy change associated with the adsorption of lysine than aspartate could arise for two reasons: first, an adsorbed lysine residue, due it is larger size, might displace more tightly bound first-layer water molecules into bulk solution than aspartate; and second, a greater number of water molecules solvate the longer (and mostly aliphatic) lysine side chain in solution and hence could be liberated upon adsorption. Remarkably, the entropic contribution to the free energy of binding for lysine is also significantly more favorable than that of arginine ($-T\Delta S_{ads} = +16 \pm 5$ kJ mol^{-1}, Table S6). This suggests that, like GolP,[33] the relative *free energies* of adsorption of lysine and arginine, calculated using GolP-CHARMM, may be different compared to the potential energies of adsorption calculated here.

The stronger-binding amino acids, histidine and arginine, were found to adsorb to the aqueous Au(111) interface via their side-chain functional groups, either adopting conformations in which only the side chain was adsorbed or those in which the side-chain and one of the two capped termini were coadsorbed (Figures 9b and S9). The guanidinium group of Arg and the protonated imidazole of HisH both preferentially

dx.doi.org/10.1021/ct301018m | J. Chem. Theory Comput. 2013, 9, 1616−1630

bound with their planes parallel to the plane of the interface, while the unprotonated imidazole ring of HisA preferentially adopted an upright conformation. Interestingly, in HisA run 5, a metastable conformation of the amino acid was identified, where along with N-terminus and side-chain adsorption, the methyl group of the capped C-terminus was also bound to the surface. This configuration, on average 30 kJ mol^{-1} higher in energy than the lowest energy HisA simulation, was stable, despite the conformation of the amino acid being distorted.

As well as reasonably reproducing experimental trends in the binding affinities of the different classes of amino acids tested here (neutral, positively and negatively charged), the absolute strength of adsorption predicted by GolP-CHARMM agrees qualitatively well with the limited experimental data available.[106] Of the two existing biointerfacial gold FFs, GolP[33,34] and CHARMM-METAL,[21,32] the original GolP FF more closely predicts the free energy of adsorption of Phe to Au(111) (ΔG = −43.6 kJ mol^{-1} for the capped amino acid[27]) relative to the experimentally determined range ($-18 < \Delta G^0 < -37$ kJ mol^{-1}). [The experimental free energy of adsorption was derived for the standard state,[107,108] whereas the calculated values were obtained for the adsorption of a single molecule without adjusting to a standard state. In practice, for the standard state chosen in ref 106, the difference should be negligible.] CHARMM-METAL, on the other hand, significantly overestimates the attraction to the surface.[21] For the amino acids simulated in this study, using both the original GolP and GolP-CHARMM FFs, the potential energy of adsorption onto the Au(111) surface was slightly less favorable for the latter set of parameters than the former (Table S6). Hence, using these data as a guide, we predict that the magnitude of the free energy of adsorption of Phe onto the Au(111) surface under aqueous conditions calculated using GolP-CHARMM to be consistent with experimental data. Therefore, although the experimental data necessary to validate GolP-CHARMM exhaustively are currently not available, we believe that our new FF is able to capture the physics and chemistry of the aqueous polypeptide−gold interface.

CONCLUSIONS

In conclusion, a new force field (FF), GolP-CHARMM, able to describe peptide adsorption at both the aqueous Au(111) and Au(100) interfaces has been derived here. The FF can reproduce the same trends in small molecule facet selectivity *in vacuo* as those observed using a systematic first-principles study employing the vdW-DF functional,[62,63] namely, a slight energetic and spatial preference for the Au(100) surface. The description of the aqueous Au(111) interface by GolP-CHARMM agrees closely with previous first-principles MD studies,[79,97] while trends in amino acid binding affinities at the same facet correlate positively with experimental data. We therefore conclude that atomistic MD simulations employing GolP-CHARMM offer a computationally accessible way to systematically study facet selectivity of peptide adsorption under aqueous conditions while accounting for the dynamic polarization of the gold atoms.

ASSOCIATED CONTENT

Supporting Information

Figures and tables, including a description of the different virtual site geometries tested for the Au(100) surface; reference and test set energetic and spatial data used to fit and validate FF parameters for both facets; snapshots of the optimal geometry of each adsorbate on Au(111) and Au(100) found from PW-DFT calculations; and additional figures detailing energetic and spatial facet selectivity of small molecule adsorption *in vacuo*, the properties of liquid water above each surface, and amino acid adsorption at the aqueous Au(111) interface. Details of GolP-TDS_{ads} calculations. This material is available free of charge via the Internet at http://pubs.acs.org.

AUTHOR INFORMATION

Corresponding Author

*E-mail: stefano.corni@nano.cnr.it; tiffany.walsh@deakin.edu.au.

Notes

The authors declare no competing financial interest.

ACKNOWLEDGMENTS

The authors gratefully acknowledge the computing facilities of CINECA and the Centre for Scientific Computing, University of Warwick. L.B.W. thanks the EPSRC for DTA studentship funding and HPC Europa2 (grant 1117_WRIGHT). This work was supported by EPSRC Programme Grant (EP/I001514/1) "Hard−Soft Matter Interfaces; From Understanding to Engineering." S.C. gratefully acknowledges funding by IIT Computational Platform under the Seed project MOPRO-SURF and by MIUR through the FIRB project Italnanonet. This work was partially supported by the Air Force Office of Scientific Research (Grant #FA9550-12-1-0226). T.R.W. thanks VESKI for an Innovation Fellowship.

REFERENCES

(1) Hnilova, M.; Khatayevich, D.; Carlson, D.; Oren, E. E.; Gresswell, C.; Zheng, S.; Ohuchi, F.; Sarikaya, M.; Tamerler, C. *J. Colloid Interface Sci.* **2012**, *265*, 97.
(2) Hnilova, M.; So, C. R.; Oren, E. E.; Wilson, B. R.; Kacar, T.; Tamerler, C.; Sarikaya, M. *Soft Matter* **2012**, *8*, 4327.
(3) Hnilova, M.; Karaca, B. T.; Park, J.; Jia, C.; Wilson, B. R.; Sarikaya, M.; Tamerler, C. *Biotechnol. Bioeng.* **2012**, *109*, 1120.
(4) Chakraborty, M.; Jain, S.; Rani, V. *Appl. Biochem. Biotechnol.* **2011**, *165*, 1178.
(5) Mahmood, M.; Casciano, D.; Xu, Y.; Biris, A. S. *J. Appl. Toxicol.* **2012**, *32*, 10.
(6) Kumar, A.; Ma, H.; Zhang, X.; Huang, K.; Jin, S.; Liu, J.; Wei, T.; Cao, W.; Zou, G.; Liang, X.-J. *Biomaterials* **2012**, *33*, 1180.
(7) Lui, J. *Phys. Chem. Chem. Phys.* **2012**, *14*, 10485.
(8) Colombo, M.; Mazzucchelli, S.; Collico, V.; Avvakumova, S.; Pandolfi, L.; Corsi, F.; Porta, F.; Prosperi, D. *Angew. Chem., Int. Ed.* **2012**, *51*, 9272.
(9) Coppage, R.; Slocik, J. M.; Briggs, B. D.; Frenkel, A. I.; Heinz, H.; Naik, R. R.; Knecht, M. R. *J. Am. Chem. Soc.* **2011**, *133*, 12346.
(10) Hnilova, M.; Khatayevich, D.; Carlson, A.; Oren, E. E.; Gresswell, C.; Zheng, S.; Ohuchi, F.; Sarikaya, M.; Tamerler, C. *J. Colloid Interface Sci.* **2011**, *365*, 97.
(11) Tamerler, C.; Khatayevich, D.; Gungormus, M.; Kacar, T.; Oren, E. E.; Hnilova, M.; Sarikaya, M. *Biopolymers* **2010**, *94*, 78.
(12) Tamerler, C.; Sarikaya, M. *ACS Nano* **2009**, *3*, 1606.
(13) Briggs, B. D.; Knecht, M. R. *J. Phys. Chem. Lett.* **2012**, *3*, 405.
(14) Hwang, L.; Chen, C. L.; Rosi, N. L. *Chem. Commun.* **2011**, *47*, 185.
(15) Auyeung, A.; Cutler, J. L.; Macfarlane, R. J.; Jones, M. R.; Wu, J. S.; Liu, G.; Zhang, K.; Osberg, K. D.; Mirkin, C. A. *Nat. Nanotechnol.* **2012**, *7*, 24.
(16) Mirau, P. A.; Naik, R. R.; Gehring, P. *J. Am. Chem. Soc.* **2011**, *133*, 18243.
(17) Ju, S.; Yeo, W.-S. *Nanotechnology* **2012**, *23*, 135701.
(18) Braun, R.; Sarikaya, M.; Schulten, K. *J. Biomat. Sci.-Polym. E.* **2002**, *13*, 747.

(19) Heinz, H.; Farmer, B. L.; Pandey, R. B.; Slocik, J. M.; Patnaik, S. S.; Pachter, R.; Naik, R. R. *J. Am. Chem. Soc.* **2009**, *131*, 9704.
(20) Heinz, H.; Jha, K. C.; Luettmer-Strathmann, J.; Farmer, B. L.; Naik, R. R. *J. R. Soc., Interface* **2010**, *8*, 220.
(21) Feng, J.; Pandey, R. B.; Berry, R. J.; Farmer, B. L.; Naik, R. R.; Heinz, H. *Soft Matter* **2011**, *7*, 2113.
(22) Vila-Verde, A.; Acres, J. M.; Maranas, J. K. *Biomacromolecules* **2009**, *10*, 2118.
(23) Vila-Verde, A.; Beltramo, P. J.; Maranas, J. K. *Langmuir* **2011**, *27*, 5918.
(24) Yu, J.; Becker, M. L.; Carri, G. A. *Small* **2010**, *6*, 2242.
(25) Yu, J.; Becker, L.; Carri, G. A. *Langmuir* **2012**, *28*, 1408.
(26) Feng, J.; Slocik, J. M.; Sarikaya, M.; Naik, R. R.; Farmer, B. L.; Heinz, H. *Small* **2012**, *8*, 1049.
(27) Hoefling, M.; Iori, F.; Corni, S.; Gottschalk, K.-E. *Langmuir* **2010**, *26*, 8347.
(28) Hoefling, M.; Iori, F.; Corni, S.; Gottschalk, K.-E. *Chem. Phys. Chem.* **2010**, *11*, 1763.
(29) Hoefling, M.; Monti, S.; Corni, S.; Gottschalk, K. E. *PLoS One* **2011**, *6*, 20925.
(30) Makarucha, A. J.; Todorova, N.; Yarovsky, I. *Eur. Biophys. J. Biophy.* **2011**, *40*, 13.
(31) Di Felice, R.; Corni, S. *J. Phys. Chem. Lett.* **2011**, *2*, 1510.
(32) Heinz, H.; Vaia, R. A.; Farmer, B. L.; Naik, R. R. *J. Phys. Chem. C* **2008**, *112*, 17281.
(33) Iori, F.; Di Felice, R.; Molinari, E.; Corni, S. *J. Comput. Chem.* **2009**, *30*, 1465.
(34) Iori, F.; Corni, S. *J. Comput. Chem.* **2008**, *29*, 1656.
(35) Jorgensen, W. L.; Maxwell, D. S.; Tirado-Rives, J. *J. Am. Chem. Soc.* **1996**, *118*, 11225.
(36) Reimers, J. R.; Wang, Y.; Cankurtaran, B. O.; Ford, M. J. *J. Am. Chem. Soc.* **2010**, *132*, 8378.
(37) Wang, Y.; Chi, Q.; Zhang, J.; Hush, N. S.; Reimers, J. R.; Ulstrup, J. *J. Am. Chem. Soc.* **2011**, *133*, 14856.
(38) Wright, L. B.; Walsh, T. R. *J. Phys. Chem. C* **2012**, *116*, 2933.
(39) Marks, L. D. *Rep. Prog. Phys.* **1994**, *57*, 603.
(40) MacKerell, A. D.; et al. *J. Phys. Chem. B* **1998**, *102*, 3586.
(41) MacKerell, A. D., Jr.; Feig, M.; Brooks, C. L., III. *J. Comput. Chem.* **2004**, *25*, 1400.
(42) Piana, S.; Lindorff-Larsen, K.; Shaw, D. E. *Biophys. J.* **2011**, *100*, 47.
(43) Collier, G.; Vellore, N. A.; Yancey, J. A.; Stuart, S. J.; Latour, R. A. *Biointerphases* **2012**, *7*, 24.
(44) Lindorff-Larson, K.; Maragakis, P.; Piana, S.; Eastwood, M. P.; Dror, R. O.; Shaw, D. E. *PLoS One* **2012**, *7*, e32131.
(45) Cino, E.; Choy, W.-Y.; Karttunen, M. *J. Chem. Theory Comput.* **2012**, *8*, 2725.
(46) Vellore, N. A.; Yancey, J. A.; Collier, G.; Latour, R. A. *Langmuir* **2010**, *26*, 7396.
(47) Barone, V.; Casarin, M.; Forrer, D.; Monti, S.; Prampolini, G. *J. Phys. Chem. C* **2011**, *115*, 18434.
(48) Mendonca, A. C. F.; Malfreyt, P.; Padua, A. A. H. *J. Chem. Theory Comput.* **2012**, *8*, 3348.
(49) Ren, P.; Ponder, J. W. *J. Phys. Chem. B* **2004**, *108*, 13427.
(50) Harten, U.; Lahee, A. M.; Toennies, J. P.; Woll, C. *Phys. Rev. Lett.* **1985**, *54*, 2619.
(51) Skoluda, P. *Electrochem. Commun.* **2004**, *6*, 785.
(52) Gibbs, D.; Ocko, B. M.; Zehner, D. M.; Mochrie, S. G. J. *Phys. Rev. B* **1990**, *42*, 7330.
(53) Mochrie, S. G. J.; Zehner, D. M.; Ocko, B. M.; Gibbs, D. *Phys. Rev. Lett.* **1990**, *64*, 2925.
(54) Ocko, B. M.; Gibbs, D.; Huang, K. G.; Zehner, D. M.; Mochrie, S. G. J. *Phys. Rev. B* **1991**, *44*, 6429.
(55) Skoluda, P. *Electrochim. Acta* **2011**, *56*, 8625.
(56) Keith, J. A.; Fantauzzi, D.; Jacob, T.; van Duin, A. C. T. *Phys. Rev. B* **2010**, *81*, 235404.
(57) Pandey, R. B.; Heinz, H.; Feng, J.; Farmer, B. L.; Slocik, J. M.; Drummy, L. F.; Naik, R. R. *Phys. Chem. Chem. Phys.* **2009**, *11*, 1989.
(58) Cohavi, O.; Reichmann, D.; Abramovich, R.; Tesler, A. B.; Bellapadrona, G.; Kokh, D. B.; Wade, R. C.; Vaskevich, A.; Rubinstein, I.; Schreiber, G. *Chem. Eur. J.* **2011**, *17*, 1327.
(59) Allen, M. P.; Tildesley, D. J. *Computer Simulation of Liquids*; Oxford University Press: Oxford, U. K., 1987.
(60) Schravendijk, P.; Ghiringhelli, L. M.; delle Site, L.; van der Vegt, N. F. A. *J. Phys. Chem. C* **2007**, *111*, 2631.
(61) Ghiringhelli, L. M.; delle Site, L. *J. Am. Chem. Soc.* **2008**, *130*, 2634.
(62) Dion, M.; Rydberg, H.; Schroder, E.; Langreth, D. C.; Lundqvist, B. I. *Phys. Rev. Lett.* **2004**, *92*, 246401−1.
(63) Thonhauser, T.; Cooper, V. R.; Li, S.; Puzder, A.; Hyldgaard, P.; Langreth, D. C. *Phys. Rev. B* **2007**, *76*, 125112.
(64) Roman-Perez, G.; Soler, J. M. *Phys. Rev. Lett.* **2009**, *103*, 096102.
(65) Hammer, B.; Hansen, L. B.; Norskov, J. K. *Phys. Rev. B* **1999**, *59*, 7413.
(66) Iori, F.; Corni, S.; Di Felice, R. *J. Phys. Chem. C* **2008**, *112*, 13540.
(67) Hong, G.; Heinz, H.; Naik, R. R.; Farmer, B. L.; Pachter, R. *ACS Appl. Mater. Interfaces* **2009**, *1*, 388.
(68) Giannozzi, P.; et al. *J. Phys.: Condens. Matter.* **2009**, *21*, 395502.
(69) Rosa, M.; Corni, S.; Di Felice, R. *J. Phys. Chem. C* **2012**, *116*, 21366.
(70) Vanderbilt, D. *Phys. Rev. B* **1990**, *41*, 7892.
(71) Perdew, J. P.; Burke, K.; Ernzerhof, M. *Phys. Rev. Lett.* **1996**, *77*, 3865.
(72) Fu, C.-L.; Ho, K.-M. *Phys. Rev. B* **1983**, *28*, 5480.
(73) Hess, B.; Kutzner, C.; van der Spoel, D.; Lindahl, E. *J. Chem. Theory Comput.* **2008**, *4*, 435.
(74) Jorgensen, W. L.; Chandrasekhar, J.; Madura, J. D.; Impey, R. W.; Klein, M. L. *J. Chem. Phys.* **1983**, *79*, 926.
(75) Neria, E.; Fischer, S.; Karplus, M. *J. Chem. Phys.* **1996**, *105*, 1902.
(76) Hockney, R. W.; Goel, S. P.; Eastwood, J. *J. Comput. Phys.* **1974**, *14*, 148.
(77) Yang, M.; Stipp, S. L. S.; Harding, J. *Crystal Growth Des.* **2008**, *8*, 4066.
(78) Heinz, H. *J. Comput. Chem.* **2010**, *31*, 1564.
(79) Cicero, G.; Calzolari, A.; Corni, S.; Catellani, A. *J. Phys. Chem. Lett.* **2011**, *2*, 2582.
(80) Langreth, D. C.; et al. *J. Phys: Condens. Matter.* **2009**, *21*, 084203.
(81) Toyoda, K.; Nakano, Y.; Hamada, I.; Lee, K.; Yanagisawa, S.; Morikawa, Y. *Surf. Sci.* **2009**, *603*, 2912.
(82) Li, G.; Tamblyn, I.; Cooper, V. R.; Gao, H.-J.; Neaton, J. B. *Phys. Rev. B* **2012**, *85*, 121409.
(83) Wellendorff, J.; Kelkkanen, A.; Mortensen, J. J.; Lundqvist, B. I.; Bligaard, T. *Top. Catal.* **2010**, *53*, 378.
(84) Lee, K.; Murray, E. D.; Kong, L.; Lundqvist, B. I.; Langreth, D. C. *Phys. Rev. B* **2010**, *82*, 081101.
(85) Wetterer, S. M.; Lavrich, D. J.; Cummings, T.; Bernasek, S. L.; Scoles, G. *J. Phys. Chem. B* **1998**, *102*, 9266.
(86) Syomin, D.; Koel, B. E. *Surf. Sci.* **2002**, *498*, 53.
(87) Kay, B. D.; Lykke, K. R.; Creighton, J. R.; Ward, S. J. *J. Chem. Phys.* **1989**, *91*, 5120.
(88) Lavrich, D. J.; Wetterer, S. M.; Bernasek, S. L.; Scoles, G. *J. Phys. Chem. B* **1998**, *102*, 3456.
(89) Syomin, D.; Koel, B. E. *Surf. Sci.* **2002**, *498*, 61.
(90) Fichthorn, K. A.; Becker, K. E.; Miron, R. A. *Catal. Today* **2007**, *123*, 71.
(91) Romaner, L.; Nobok, D.; Puschnig, P.; Zojer, E.; Ambrosch-Draxl, C. *New J. Phys.* **2009**, *11*, 053010.
(92) Syomin, D.; Kim, J.; Koel, B. E.; Ellison, G. B. *J. Phys. Chem. B* **2001**, *105*, 8387.
(93) Makov, G.; Payne, M. C. *Phys. Rev. B* **1995**, *51*, 4014.
(94) Skelton, A. A.; Liang, T. N.; Walsh, T. R. *ACS Appl. Mater. Interfaces* **2009**, *1*, 1482.
(95) Jena, K. C.; Hore, D. K. *Phys. Chem. Chem. Phys.* **2010**, *12*, 14383.

(96) Schneider, J.; Colombi-Ciacchi, L. *J. Am. Chem. Soc.* **2012**, *134*, 2407.
(97) Nadler, R.; Sanz, J. F. *J. Chem. Phys.* **2012**, *137*, 114709.
(98) Meng, M.; Stievano, L.; Lambert, J.-F. *Langmuir* **2004**, *20*, 914.
(99) Schnur, S.; Gross, A. *New J. Phys* **2009**, *11*, 125003.
(100) Lin, X.; Gross, A. *Surf. Sci.* **2012**, *606*, 886.
(101) Grimme, S. *J. Comput. Chem.* **2006**, *27*, 1787.
(102) Klimes, J.; Bowler, D. R.; Michaelides, A. *Phys. Rev. B* **2011**, *83*, 195131.
(103) Pan, L.; Jung, S.; Yoon, R.-H. *J. Colloid Interface Sci.* **2011**, *2361*, 321.
(104) Peelle, B. R.; Krauland, E. M.; Wittrup, K. D.; Belcher, A. M. *Langmuir* **2005**, *21*, 6929.
(105) Hnilova, M.; Oren, E. E.; Seker, U. O. S.; Wilson, B. R.; Collino, S.; Evans, J. S.; Tamerler, C.; Sarikaya, M. *Langmuir* **2008**, *24*, 12440.
(106) Li, H.-Q.; Chen, A.; Roscoe, S. G.; Lipkowski, J. *J. Electroanal. Chem.* **2001**, *500*, 299.
(107) Jastrzebska, J.; Jurkiewicz-Herbich, M.; Trasatti, S. *J. Electroanal. Chem.* **1987**, *216*, 21−28.
(108) Wei, Y.; Latour, R. A. *Langmuir* **2008**, *24*, 6721−6729.